D. Nouailhas and G. Cailletaud**

Multiaxial Behaviour of Ni-Base Single Crystals

REFERENCE Nouailhas, D. and Cailletaud, G., **Multiaxial behaviour of Ni-base single crystals,** *Multiaxial Fatigue and Design*, ESIS 21 (Edited by A. Pineau, G. Cailletaud, and T. C. Lindley) 1996, Mechanical Engineering Publications, London, pp. 75–82.

ABSTRACT This paper is an extended summary, revisiting several studies on the macroscopic behaviour of single crystal superalloys under torsion or tension–torsion loadings. We would like to emphasize that the relative orientation of the loading and of the crystallographic axes changes along the circumference, so that strain and stress are heterogeneous in the specimen. Typical results are then collected, both from the theory (including FE computations), and from tests performed at room temperature, using microstrain gauges for local strain measurement.

1 Introduction

Tension–torsion tests were extensively used in the last ten years to produce multiaxial data. This was also made for single crystals (**1, 2**). Two types of approaches were used to model these tests, the first one introducing a macroscopic criterion for cubic crystals, *id est* a specific version of the Hill criterion with only one adjustable coefficient (**3–5**), the second one using the Schmid law and crystallographic plasticity (**6–9**). The second type of approach, which is physically supported, shows that, due to the relative orientation of the shear load and of the crystallographic axes, the strain and stress should be heterogeneous along the circumference. This fact is ignored by the macroscopic quadratic criteria, which predict that the strain and stress fields are uniform if the ⟨001⟩ axis is parallel to the axis of the tube: additional invariants have then to be considered in this kind of model (**10**). Surprisingly, this was also forgotten by most of the authors in the analysis of their experimental results. The cause defended in this paper is that torsion tests on single crystals can only be analysed by means of FE computations (**11, 12**). It is then pointed out that the global response in terms of couple and angle may be successfully represented with a wrong model, and that only the comparison of the local shear is significant. For the case of pure torsion, this comparison should be made in the soft zones in the ⟨110⟩ regions, where the shear load direction exactly follows the slip direction.

*Onera, 29 av. de la Division Leclerc, BP 72, 92322 Châtillon Cedex, France.
†Centre des Matériaux, Ecole des Mines de Paris, URA CNRS 866, BP 87, 91003 EVRY Cedex, France.

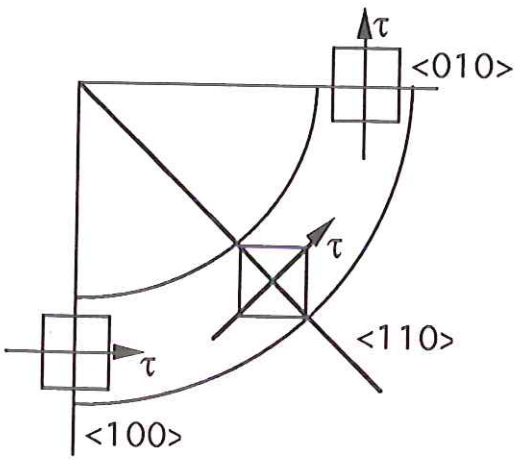

Fig 1 Relative orientation of shear and of the crystallographic axes in a thin tube subjected to a torsion loading.

2 Theoretical Results

2.1 *Basic results deduced from Schmid law*

Cube slip operates on the directions ⟨011⟩ in {001} planes, and octahedral slip on ⟨011⟩ in {111} planes. In both cases, as shown in Fig. 1, the shear loading τ generates a lower resolved stress in the region corresponding to the crystallographic axes ⟨001⟩ and ⟨010⟩, for a ⟨001⟩ oriented tube, compared with the ⟨110⟩ zone, for which τ is colinear to the slip direction. As a matter of fact, the Schmid factor in shear is equal to 1 for one of the cube systems and $1/\sqrt{2}$ for two octahedral systems for that location. The two types of systems may be active or not, depending on the respective values of the critical shear stress on each system family. The situation becomes more complex in the case of tension–torsion loading. The slip activity has to be checked on the yield surface, which has a different shape in ⟨100⟩ and in ⟨110⟩ zone. This is illustrated in Fig. 2(c), showing that, according to the value of τ/σ ratio, cube or octahedral slip may be predominant. The discussion on this last point will be made below, and supported by FE computations. These computations are made with the crystallographic model presented in the next section.

2.2 *Expression of the model*

It is a crystallographic model derived from Schmid law, assuming that crystallographic slip is the only micromechanical mechanism producing a significant macroscopic strain. It is adapted to the specific case of nickel-base

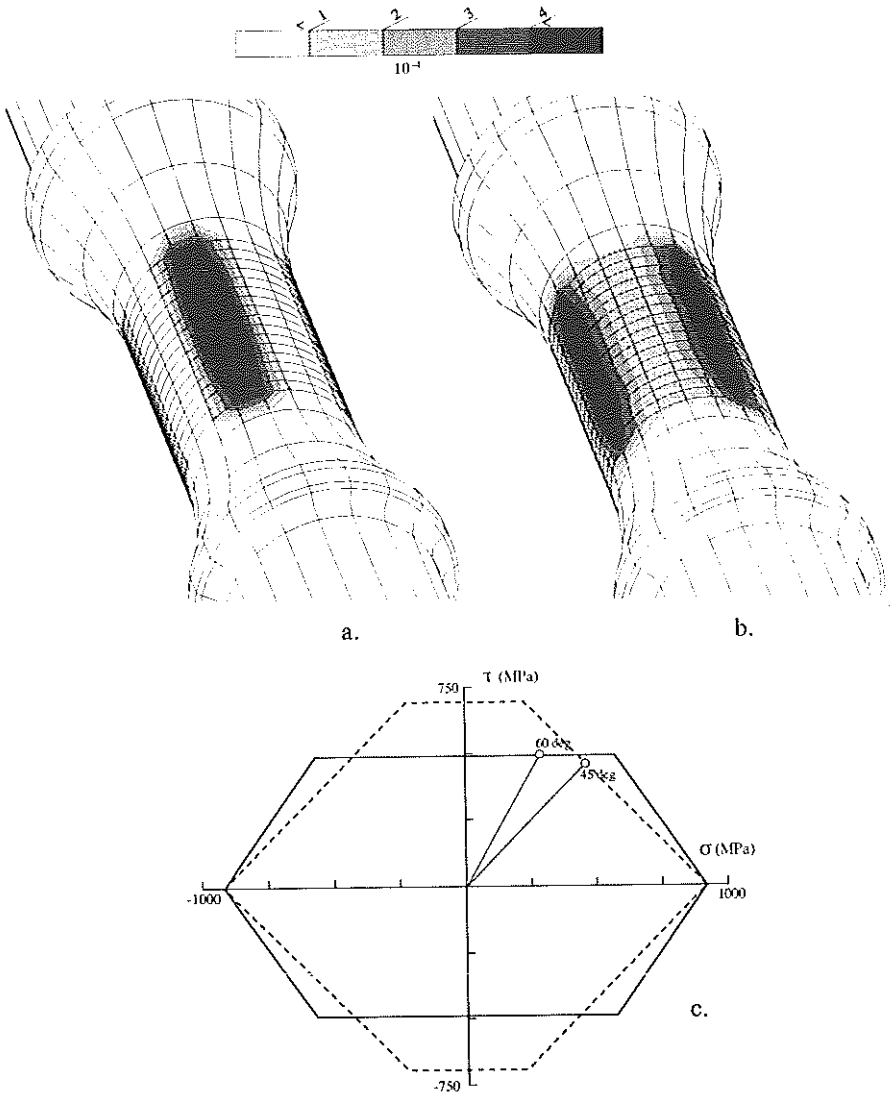

Fig 2 Location of the plastic zones at the onset of plastic flow for two shear/tension ratios: (a) $\tau/\sigma = 1.732$; (b) $\tau/\sigma = 1$; (c) yield surface in ⟨110⟩ and ⟨100⟩ regions. — Schmid criterion in ⟨110⟩ -- Schmid criterion in ⟨100⟩ ($\tau_{octa.} = 375$ MPa; $\tau_{cube} = 490$ MPa)

single crystals, for which two slip system families are active, cube and octahedral slip. The equations for the inelastic part of the crystallographic model are given as equations (1–4). The critical variable producing plastic strain is the resolved shear stress, computed from the orientation tensor **m** equation (1). Two

hardening variables are introduced for each system, kinematic (x^s) and isotropic (r^s). As shown in equation (2), this second variable accounts for coupling between the various systems, by means of an interaction matrix (h). Both of them are used in the definition of a linear threshold function, which corresponds to a generalization of the Schmid law.

$$\tau^s = \sigma_{ij} m^s_{ij} \qquad \text{with } m^s_{ij} = \frac{1}{2}(n^s_i l^s_j + n^s_j l^s_i) \tag{1}$$

$$x^s = c_1 \alpha^s \qquad \text{and } r^s = r_{01} + q_1 \sum_j h_{sj}(1 - e^{-b_1 v^j}) \tag{2}$$

$$\text{if } f^s > 0 \qquad (\text{with } f^s = |\tau^s - x^s| - r^s): \qquad \dot{v}^s = \left\langle \frac{f^s}{k_1} \right\rangle^{n_1} \tag{3}$$

$$\dot{\gamma}^s = \dot{v}^s \operatorname{sign}(\tau^s - x^s); \qquad \dot{\alpha}^s = \dot{\gamma}^s - d_1 \alpha^s \dot{v}^s; \qquad \dot{\varepsilon}^p_{ij} = \sum_s \dot{\gamma}^s m^s_{ij} \tag{4}$$

If the applied resolved stress is located outside the elastic domain, the approach assumes that a viscoplastic slip will appear on the system, classically computed from the distance to the threshold by means of a power function, equation (3). The v^s variable is the accumulated slip for the system s and defines the isotropic hardening. From v^s, one can compute the shear strain rate $\dot{\gamma}^s$ and the kinematic hardening rate $\dot{\alpha}^s$. The strain rate tensor is then obtained by summing up the non-zero strain rates, as shown in equation (4). In these constitutive equations, for each slip system family (I = 1, 2, ...), the coefficients k_I and n_I account for viscosity, the coefficients c_I and d_I the kinematic hardening, then r_{0I}, q_I, b_I and the (h) matrix the isotropic hardening, which is simply diagonal in the present case (if $i = j$, $h_{ij} = 1$). Their values are listed below for the material used (CMSX2), the indices 1 and 2 standing respectively for octahedral and cube slip. It has to be noted that, due to the choice of low k_I values, the model is practically rate-insensitive. The elastic part of total strain is classically modelled by a macroscopic relation between stress and strain tensors, through an elastic tensor for cubic elasticity.

The material coefficients used for the CMSX2 at room temperature (MPa s) are as follows.

Viscosity: $n = 12$ $K_1 = 46$ $K_2 = 55$
Initial critical shear stress: $r_{01} = 265$ $r_{02} = 345$
Isotropic hardening: $q_1 = 98$ $q_2 = 127$ $b_1 = 13$ $b_2 = 6.4$
Kinematic hardening: $c_1 = 372217$ $d_1 = 39187$ $c_2 = 343232$ $d_2 = 5954$

2.2 *Finite-element computations under tension–torsion loading*

The results obtained for two finite-element computations are reported in Fig. 2. The yield surface is deduced from experimental measurements **(14)**, so that

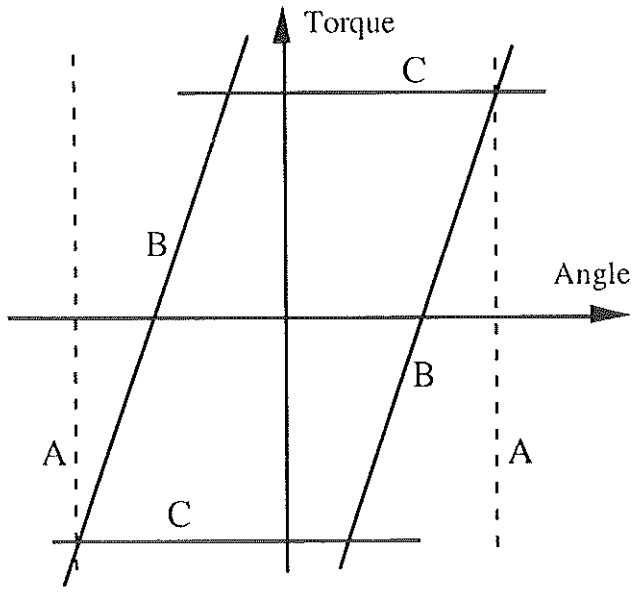

Fig 3 How to build a good global torque–angle curve from a false model.

the apparent critical resolved shear stresses are higher than the initial values listed above which correspond to a zero offset. At least these computations illustrate that for torsion predominant loadings (e.g. 60° in the σ–τ plane), the critical zone corresponds to the ⟨110⟩ regions, the critical systems being cube systems. When tension becomes predominant, the critical zone is along ⟨100⟩, and the critical slip is octahedral slip. Complex stress redistributions are associated with this heterogeneity, so that the experimental determination of the yield surface has to be made carefully: in ⟨110⟩ regions, the onset of plastic flow for paths involving a predominant tension loading may be influenced by the plastic flow in the ⟨100⟩ direction, which starts first, the inverse effect being true for predominant torsion loadings in ⟨100⟩ regions.

Figure 2 illustrated the idea that the global response is the result of complex local phenomena. It follows that this information may be too poor. This is shown in Fig. 3, which illustrates the fact that the angle–torque response of a tubular specimen will be correctly represented with any kind of model (even a bad one), provided it captures the ultimate stress of the loading curve. As the tests are usually performed under angle control, the boundaries A of the cycle are correct. If the elastic properties are well characterized and the rigidity of the grip system well known (or if there is a local measurement of the angle on the cylindrical part of the specimen), the slope B will be correct too. The only value depending on (visco)plastic behaviour is the torque value during the plastic

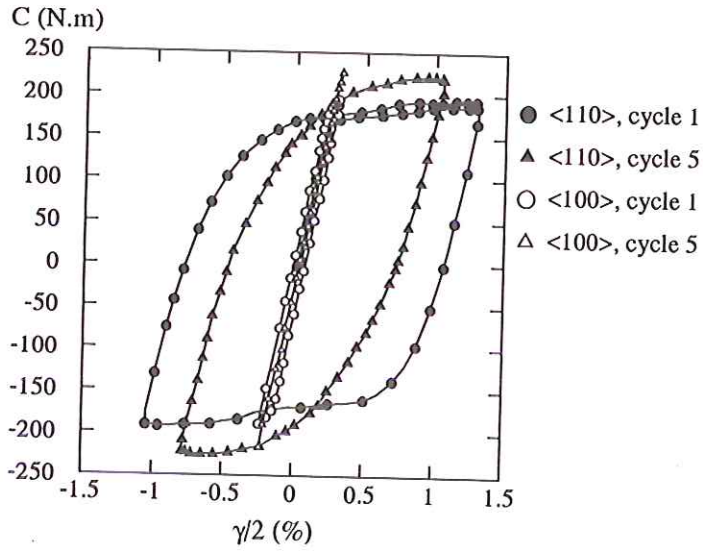

Fig 4 Evolution of the torque *vs* local shear strain in ⟨100⟩ and ⟨110⟩ regions (results from strain gauge measurement).

regime. It is usually observed under one-dimensional loading that the behaviour is strongly nonlinear, and that the stress–strain loop quickly reaches an asymptotic value in terms of stress during plastic flow. That means that the prediction of C-level in Fig. 3 will be correct provided that this asymptotic value is correctly reproduced in the model.

In particular, the global response predicted by a model with a quadratic criterion will be in good agreement with the experimental torque–angle curve. This cannot demonstrate that the model is good. The most serious error made in the literature is then to find a good agreement between such a (wrong) model and a (wrong) local experimental response, deduced from the global one, assuming that stress and strain are uniform along the circumference.

3 Local Strain Evolution in a Pure Torsion Test

3.1 *Experiment*

Pure torsion tests are performed at room temperature on CMSX2 alloy. The specimen used is a thin-walled tube grown along ⟨001⟩ crystallographic orientation. Inside and outside diameters are 14 and 16 mm respectively, and the length of the cyclindrical part is 24 mm. Two strain gauge microrosettes are attached in the ⟨100⟩ and ⟨010⟩ secondary orientations, which were initially localized by Laue X-ray back reflection method (**13, 14**). The analysis of the slip traces revealed that cube slip is predominant, even at room temperature, and that slip is more intense in the ⟨110⟩ zones.

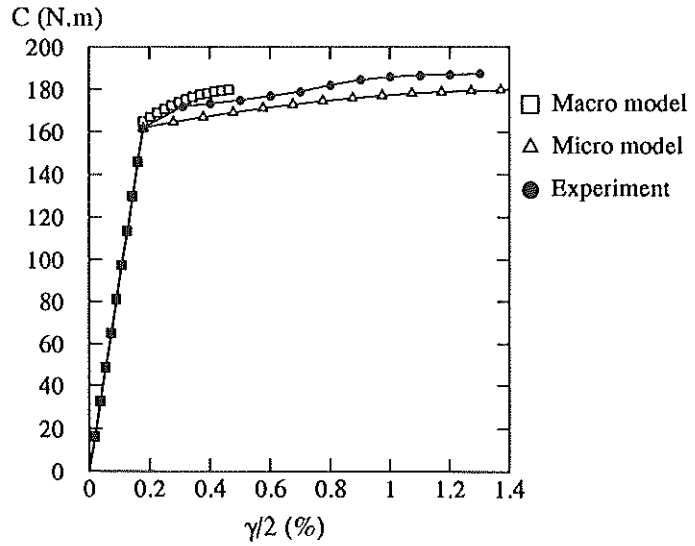

Fig 5 Simulation of the local responses with a Hill-type model and with the crystalline model.

The curves reported in Fig. 4 allow to quantify the heterogeneity. Four loops are shown: as no local stress measurement is available, the global torque is plotted on the vertical axis. The material exhibits cyclic hardening, so that the width of the loop decreases between the first cycle and cycle number 5, which more or less corresponds to the mechanical steady-state. For the ⟨100⟩ zone, the amount of plasticity is very low at the first cycle, and the stabilized cycle is elastic. For the ⟨110⟩ zone, the plasticity is about twenty times higher than for ⟨100⟩ at the first cycle, and remains very large after 5 cycles.

3.2 *Numerical simulation*

A finite-element computation is needed to determine the simulated response in terms of torque and local strain. It is performed with the single crystal model implemented in the Zebulon code (**11**). A comprehensive study of the results is given in (**14**). Figure 5 illustrates the key result. The diagram shown is restricted to the first torsion loading, for the sake of clarity. The local simulated response is obtained from the node located on the outside diameter, at 45° between ⟨100⟩ and ⟨010⟩. It is in good agreement with the experiment. On the other hand, the same figure shows the local curve obtained with a Hill type model, identified to give the same results as the crystallographic model in tension along ⟨100⟩ and ⟨111⟩ regions (**13**). It is not surprising to observe that the predicted response with this model underestimates the experimental strain.

4 Conclusion

A thin-tube specimen made of single crystal cannot be considered as a volume element, but as a structure. As the stress redistributions are complex, it may be dangerous also to use simplified methods, with uniform stress and strain assumptions, and full FE computations must be performed for the analysis of the tests. It is also worth noting that considering a uniform strain distribution leads to underestimating the experimentally observed local strains.

References

(1) JORDAN, E. H. and WALKER, K. P. (1985) Biaxial constitutive modelling and testing of a single crystal superalloy at elevated temperature, *1st Conf. on Multiaxial Fatigue*, Sheffield.
(2) HASEBE, T., MASAO, S. and OHNAMI, M. (1994) Constitutive relation of nickel-base single crystal superalloy CMSX2 under multiaxial loading, *4th Int. Conf. on Biaxial Multiaxial Fatigue*, Saint Germain en Laye, France, May 31-June 3.
(3) LEE, D. and ZAVERL, F. (1978) A generalized strain rate dependent constitutive equation for anisotropic metals, *Acta Met. Mater.*, **26**, p. 1771.
(4) CHOI, S. H. and KREMPL, E. (1989) Viscoplasticity theory based on overstress applied to the modeling of cubic single crystals, *Eur. J. of Mechanics A/Solids*, **8**, p. 219.
(5) NOUAILHAS, D. and, FREED, A. D. (1992) A viscoplastic theory for anisotropic materials, *J. of Engng. Mat. Tech.*, **114**, p. 97.
(6) DAME, L. T. and STOUFFER, D. C. (1988) A crystallographic model for nickel-base single crystal alloys, *ASME J. of Appl. Mech.*, **55**, p. 325.
(7) MERIC, L., POUBANNE, P. and CAILLETAUD, G. (1991) Single crystal modeling for structural calculations, Part 1: model presentation, *J. of Engng. Mat. and Techn.*, **113**, p. 162.
(8) JORDAN, E. H. and WALKER, K. P. (1992) A viscoplastic model for single crystals, *J. of Engng Mat. Techn.*, **14**, p. 19.
(9) OHNO, N., MIZUNO, T., KAWAJI, H. and OKADA, I. (1992) Multiaxial creep of a nickel-base directionally solidified alloy: anisotropy and simulation, *Acta Met. Mater.*, **40**, p. 559.
(10) NOUAILHAS, D. and CAILLETAUD, G. (1992) Comparaison de divers critères anisotropes pour monocristaux cubiques a faces centrees (CFC), Note aux Comptes Rendus de l'Académie des Sciences de Paris, t. 315, Serie II, p. 1573.
(11) MERIC, L. and CAILLETAUD, G. (1991) Single crystal modeling for structural calculations, Part 2: finite element implementation, *ASME J. of Engng Mat. Techn.*, **113**, p. 171.
(12) NOUAILHAS, D., CULIE, J. P., MERIC, L. and CAILLETAUD, G. (1992) Finite element analysis of the stress-strain behaviour of single crystal tubes, *Proc. Mecamat 92, Int. Seminar on Multiaxial Plasticity*, Sept. 1–4.
(13) NOUAILHAS, D., PACOU, D., CAILLETAUD, G., HANRIOT, F. and REMY, L. (1993) Experimental study of the anisotropic behavior of the CMSX2 single crystal superalloy under tension–torsion loadings, *Proc. ASTM Symp. on Multiaxial Fatigue*, San Diego, (1991); in *Advances in Multixial Fatigue*, **ASTM STP 1191**, eds., D. L., McDowell and R., Ellis, p. 244.
(14) NOUAILHAS, D. and CAILLETAUD, G. (1995) Tension–torsion behavior of single crystal superalloys: experiment and finite element analysis, *Int. J. of Plasticity*, **11**, p. 451.